Supporting Information

Hierarchical superhydrophilic/superaerophobic CoMnP/Ni₂P nanosheets-based microplates arrays for enhanced overall water splitting

Mengzhao Liu,‡[a] Zhe Sun,‡[a] Shiyan Li,‡[b,c] Xiaowa Nie,‡[a] Yuefeng Liu,[b] Erdong Wang,[b] and Zhongkui Zhao*[a]

[a]State Key Laboratory of Fine Chemicals, Department of Catalysis Chemistry and Engineering, School of Chemical Engineering, Dalian University of Technology, Dalian 116024, P.R. China

[b]Dalian National Laboratory for Clean Energy (DNL), Dalian Institute of Chemical Physics, Chinese Academy of Sciences, Dalian 116023, P.R. China

[c]University of Chinese Academy of Sciences, Beijing 100049, China.

§This author contributed equally to this work

*E-mail: zkzhao@dlut.edu.cn

Table of Contents

1. Supplementary Figures

2. Supplementary Tables

3. References

1. Supplementary Figures
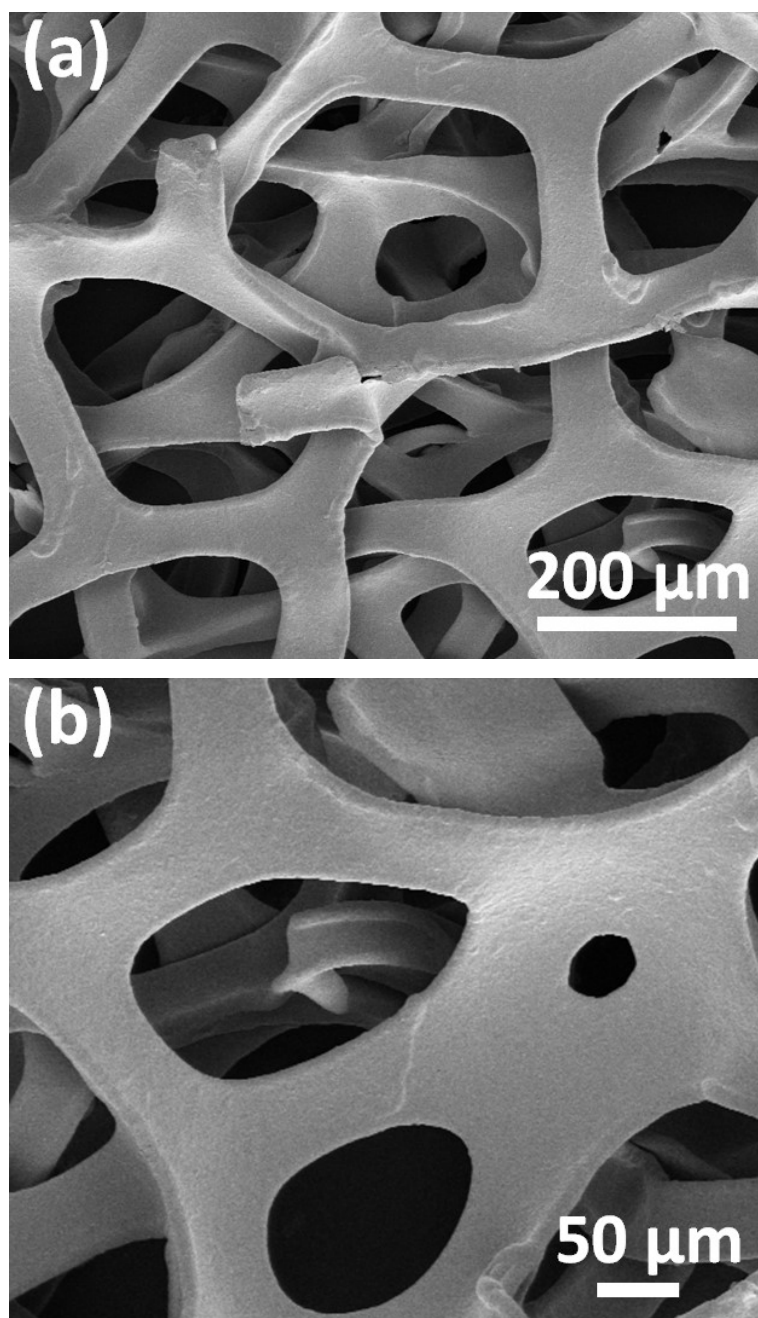
Fig. S1 SEM images of bare Ni foam with different magnification factors: (a) Low resolution and (b) High resolution.
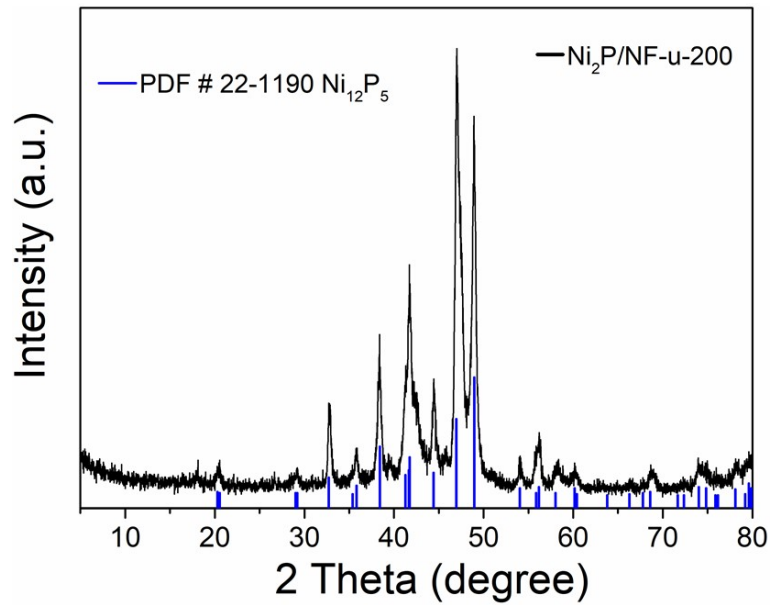
Fig. S2 XRD patterns of Ni$_2$P/NF-u-200.

The hydrothermal process in the presence of red P but absence of urea (or the added urea is not more than 200 mg) leads to a strongly acidic solution and at the same time the PH$_3$ is produced (Eq. 1). The metal Ni of Ni foam reacts with H$^+$ to produce Ni^{2+} (Eq. 2). As a result, the immersed NF is completely broken and then disappears, and also we see the formation of some precipitate. The XRD pattern of Ni$_2$P/NF-u-200 confirms that the resulting precipitate is Ni$_{12}$P$_5$ phase (PDF # 22-1190). The phosphorization process can be proposed as Eq. 3.

$$8P + 12H_2O \rightarrow 5PH_3 + 9H^+ + 3PO_4^{3-} \quad \text{(1)}$$

$$Ni + 2H^+ \rightarrow Ni^{2+} + H_2 \quad \text{(2)}$$

$$96Ni^{2+} + 49PH_3 + 36H_2O \rightarrow 8Ni_{12}P_5 + 219H^+ + 9PO_4^{3-} \quad \text{(3)}$$
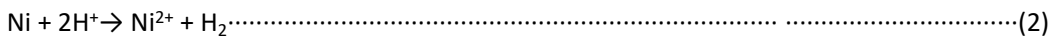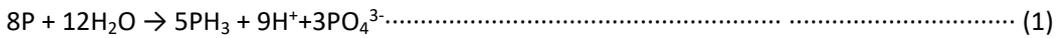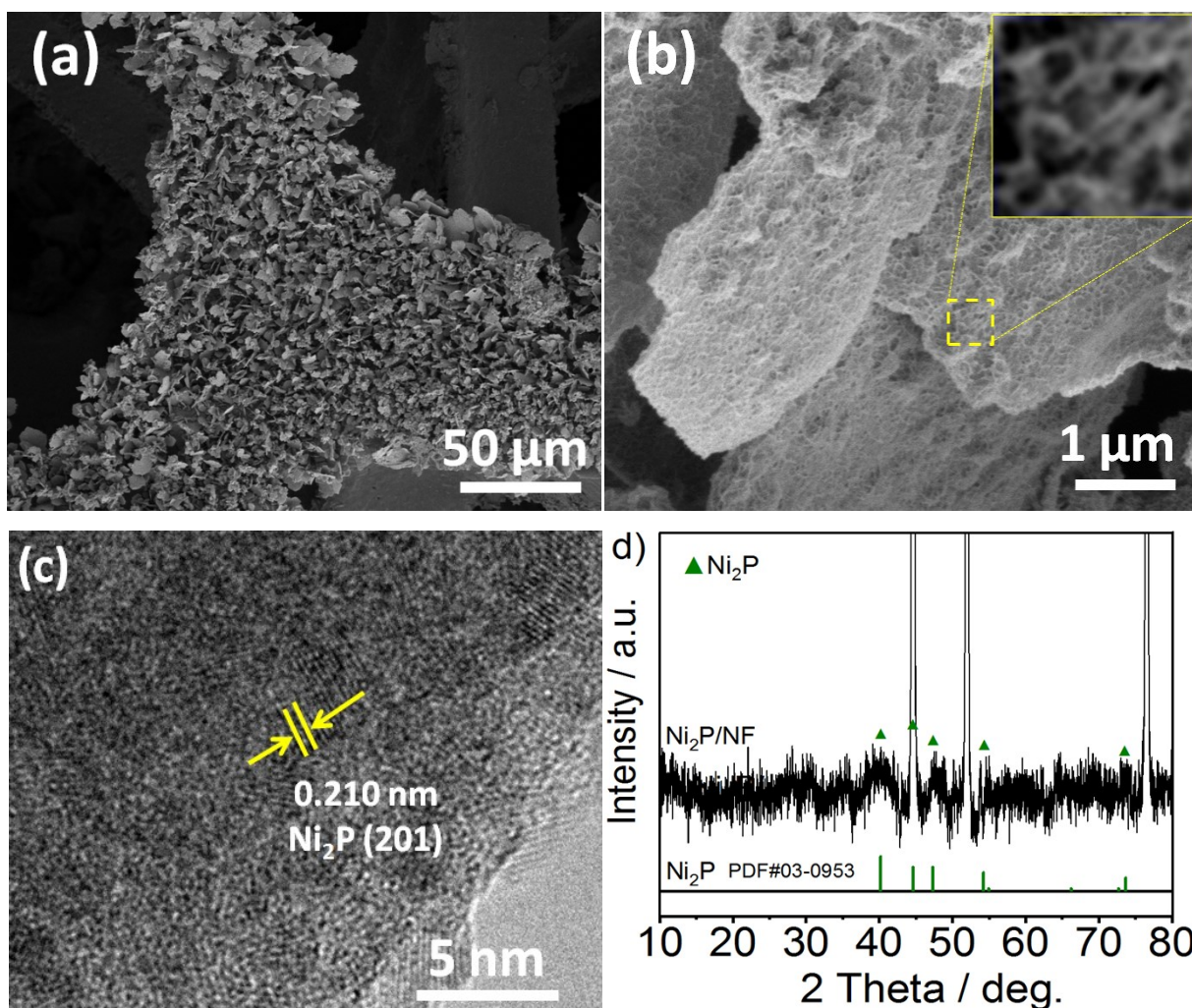
Fig. S3 (a,b) SEM, (c) HRTEM images, and (d) XRD pattern of Ni$_2$P/NF-600.

If the urea amount was further increased from 200 mg to 600 mg, the Ni foam can be well maintained. Interestingly, the hierarchical arrays on Ni foam have been formed (Fig. S3a,b). The HRTEM image (Fig. S3c) and XRD pattern (Fig. S3d) of Ni$_2$P/NF-600 show that the as-formed arrays are Ni$_2$P phases, besides the metal Ni of Ni foam, the Ni$_2$P phase is clearly confirmed. To analyze this process, the addition of more amount of urea can produce a large amount of OH$^-$under hydrothermal condition (Eq. 4), which can neutralize the H$^+$(Eq. 5) that is formed from the hydrolysis of red P under hydrothermal condition (Eq. 1). The reaction of the metallic Ni with acid (Eq. 2) can be weakened. As a result, different from the situation with small amount of urea, when 600 mg urea was added in the red P-containing hydrothermal system, the structure of Ni foam can be well kept. More interestingly, the hierarchical Ni$_2$P arrays grow on the Ni foam. It can be proposed that more OH$^-$ from urea hydrolysis promotes the formation of PH$_3$ from red P hydrolysis (Eq. 1), which leads to the formation of Ni$_2$P via the reaction of Eq. 16 rather than the Ni$_{12}$P$_5$ phase that was formed under the low-urea phosphorization condition (Eq. 3).

$$CO(NH_2)_2 + 3H_2O \rightarrow CO_2 + 2NH_4^+ + 2OH^- \cdots\cdots\cdots\cdots\cdots\cdots\cdots\cdots\cdots(4)$$

$$H^+ + OH^- \rightarrow H_2O \cdots\cdots\cdots\cdots\cdots\cdots\cdots\cdots\cdots\cdots (5)$$

$$16Ni^{2+} + 9PH_3 + 4H_2O \rightarrow 8Ni_2P + 35H^+ + PO_4^{3-} \cdots\cdots\cdots\cdots\cdots\cdots\cdots\cdots \cdots\cdots (6)$$
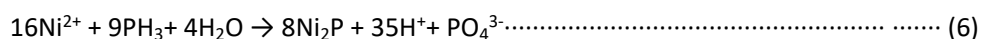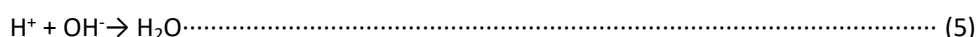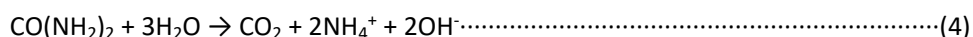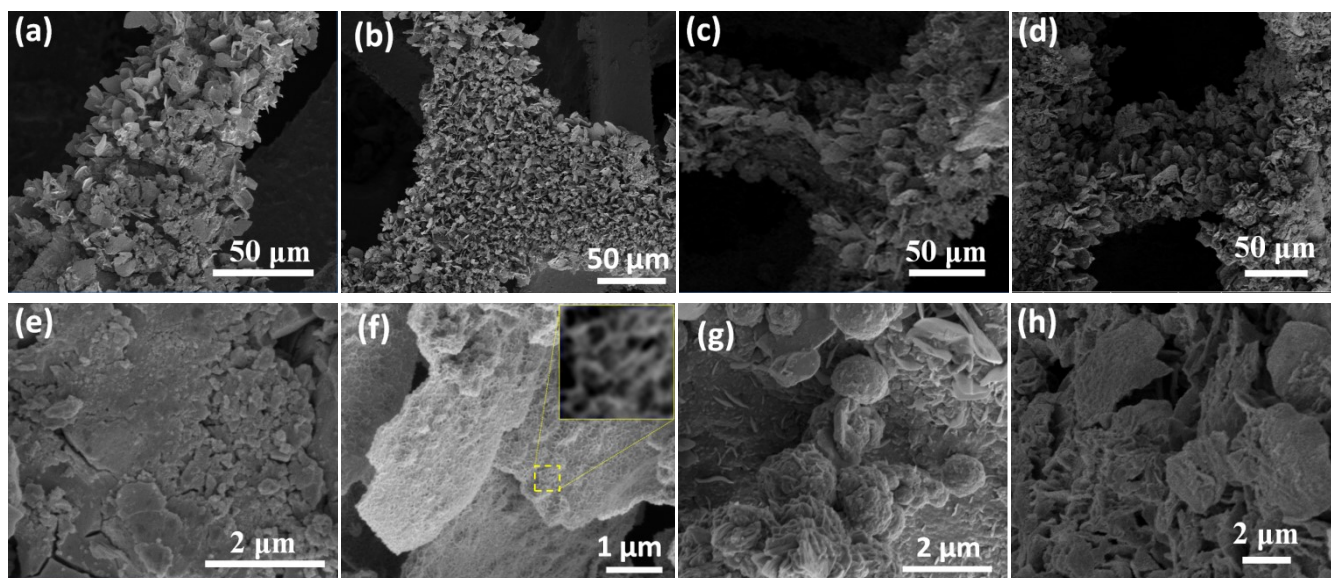
Fig. S4 SEM images of (a,e) Ni$_2$P/NF-u-400, (b,f) Ni$_2$P/NF-u-600, (c,g) Ni$_2$P/NF-u-800, and (d,h) Ni$_2$P/NF-u-1000.

The added urea acts as a modulating agent for the synthesis of metal phosphide in the developed urea-modulated hydrothermal phosphorization process using red P as P source. As is mentioned as above, the hydrolysis of urea (Eq. 4) can efficiently modulate both the acidic properties of aqueous solution and hydrolysis process of red P (Eq.1) under hydrothermal condition. As a result, the dissolution of metallic Ni from Ni foam to Ni^{2+}and the further phosphorization of Ni^{2+} to Ni$_2$P can be adjusted. By varying the amount of added urea in the hydrothermal phosphorization process, a series of Ni$_2$P/NF-u-*m* with diverse morphologies have been prepared (Fig. S4). Ni foam not only acts as a robust support for hierarchical Ni$_2$P/NF-u-m arrays but also provides Ni sources for the growth of Ni$_2$P arrays on Ni foam. By using 400 mg urea, although the Ni foam can be well kept, the grown Ni$_2$P on NF features a mixture of sheets and particles (Fig. S4a,e). Increasing urea dosage from 400 to 600 mg, the hierarchical Ni$_2$P arrays on NF are prepared (Fig. S4b,f). If the amount of urea was further increased, the aggregated Ni$_2$P plates rather than hierarchical Ni$_2$P arrays can be formed (Fig. S4c, d, g, h).
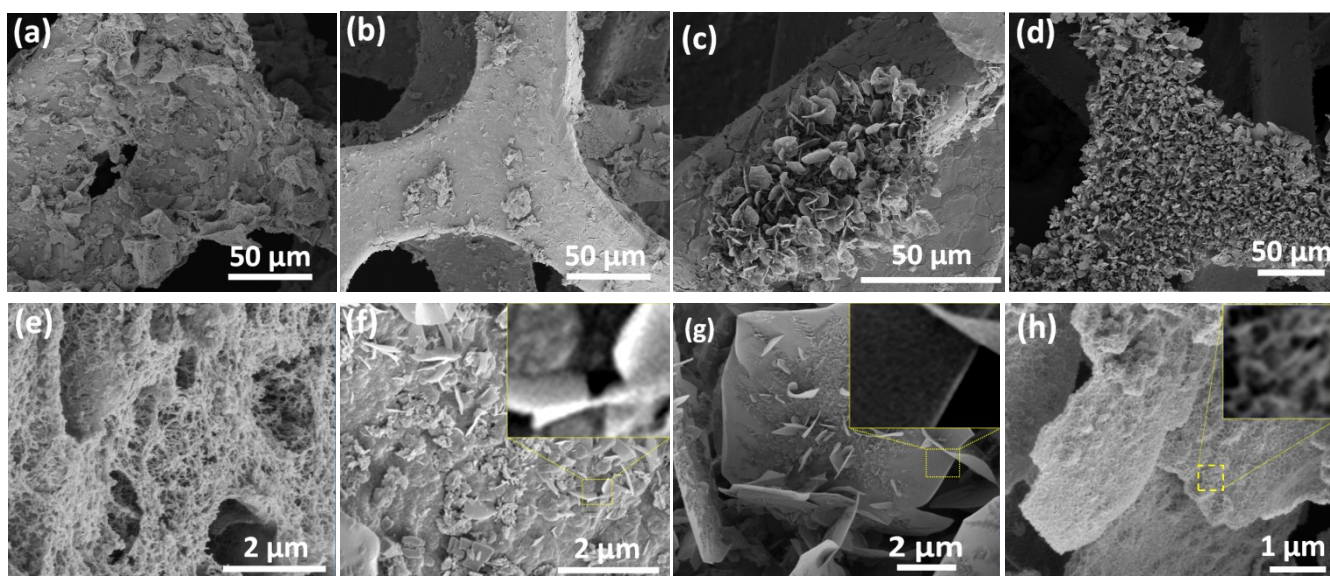
Fig. S5 SEM images of Ni$_2$P/NFsamples prepared by using diverse hydrothermal times: (a,e) 6 h; (b,f) 12 h; (c,g) 18 h; (d,h) 24 h.

Fig. S5 presents the evolution of hierarchical Ni$_2$P arrays on NF through the urea-modulated hydrothermal phosphorization strategy. While the hydrothermal phosphorization process is performed for 6 h, the filamentous Ni$_2$P grows on NF (Fig. S5a,e). With the extending hydrothermal time up to 12 h, some Ni$_2$P hierarchical nanostructures featuring submicroplates composed of nanosheets begin to form. Besides a few plate-like Ni$_2$P hierarchical architecture, and a large amount of Ni$_2$P particles can be observed (Fig. S5b,f). The further extending hydrothermal time leads to the formation of more and more hierarchical Ni$_2$P arrays (Fig. S5c,d,g,h). From Fig. S5d,h, the hierarchical Ni$_2$P arrays on NF can be formed while the hydrothermal phosphorization process is performed for 24 h.
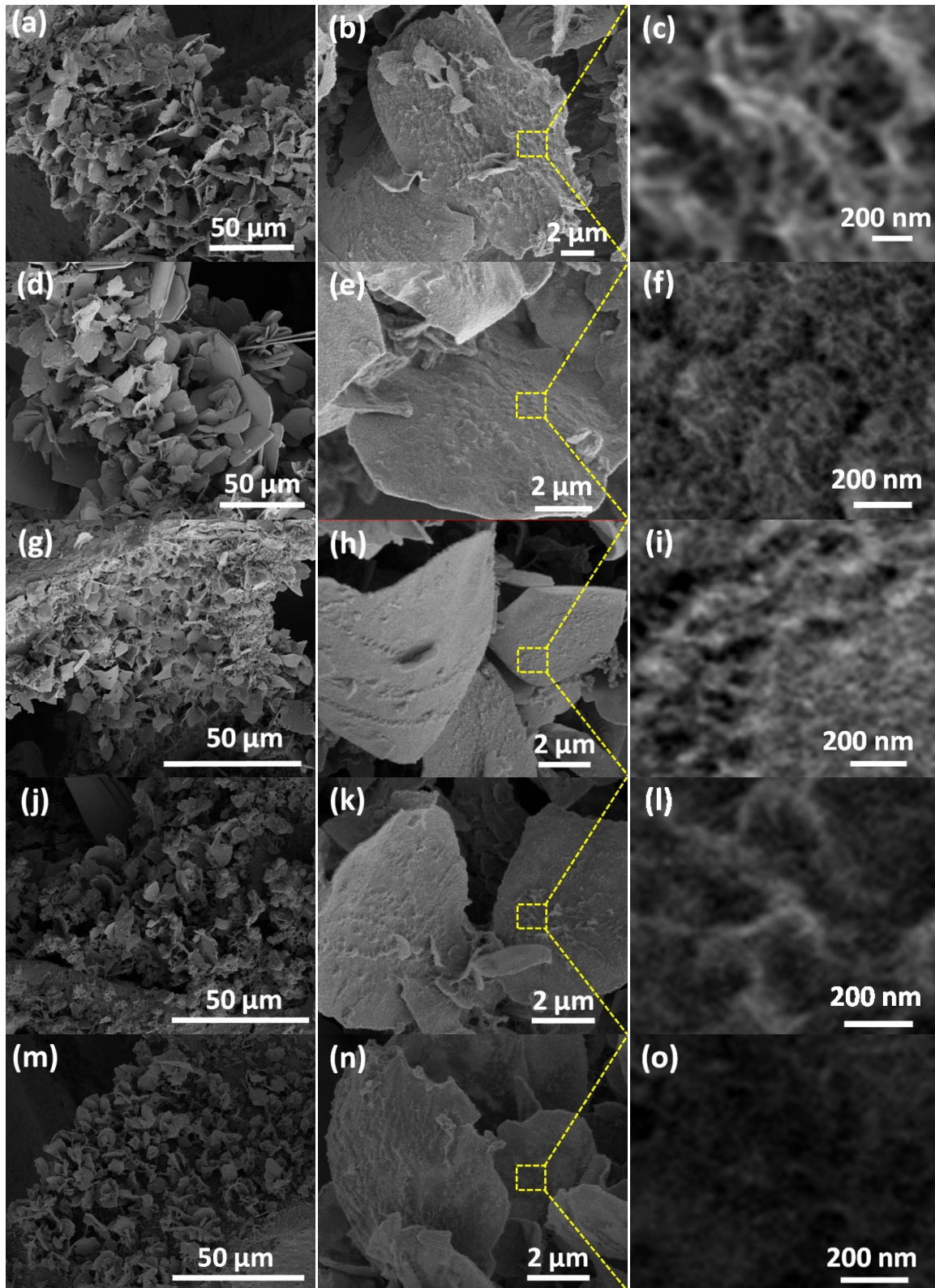
Fig. S6 SEM images of (a-c) CoMnP/Ni$_2$P-NF-31, (d-f) CoMnP/Ni$_2$P-NF-21, (g-i) CoMnP/Ni$_2$P-NF-11, (j-l) CoMnP/Ni$_2$P-NF-12, and (m-o) CoMnP/Ni$_2$P-NF-13.

Based on the aforementioned discussion, the CoP and MnP can be produced through the reactions of Co^{2+} and Mn^{2+} with PH$_3$ (Eq. 7 and 8), which are modulated by the added urea (Eq. 4, 5).

$$2Co^{2+} + 6PH_3 + 16H_2O \rightarrow 2CoP + 16H^+ + 4PO_4^{3-} + 17\ H_2 \cdots\cdots\cdots\cdots\cdots\cdots\cdots\cdots\cdots\cdots\cdots\cdots\cdots\cdots\cdots\ (7)$$

$$2Mn^{2+} + 6PH_3 + 16H_2O \rightarrow 2MnP + 16H^+ + 4PO_4^{3-} + 17\ H_2 \cdots\cdots\ \cdots\cdots\ \cdots\cdots\ \cdots\cdots\ \cdots\cdots\ \cdots\cdots\ \cdots\cdots\ \cdots\cdots\ \cdots\cdots\ \cdots\cdots\ (8)$$
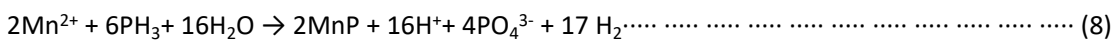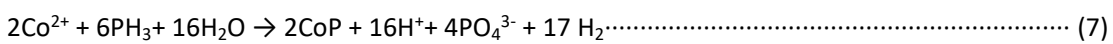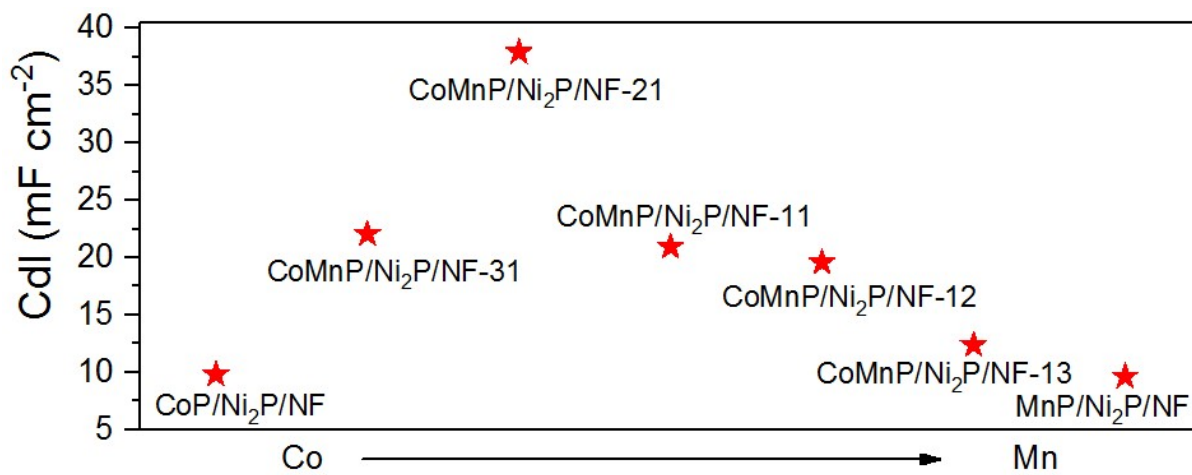
Fig. S7 The double layer capacitances (Cdl) of CoP/Ni$_2$P/NF, CoMnP/Ni$_2$P/NF-31, CoMnP/Ni$_2$P/NF-21, CoMnP/Ni$_2$P/NF-11, CoMnP/Ni$_2$P/NF-12, CoMnP/Ni$_2$P/NF-13, MnP/Ni$_2$P in 1 M KOH.
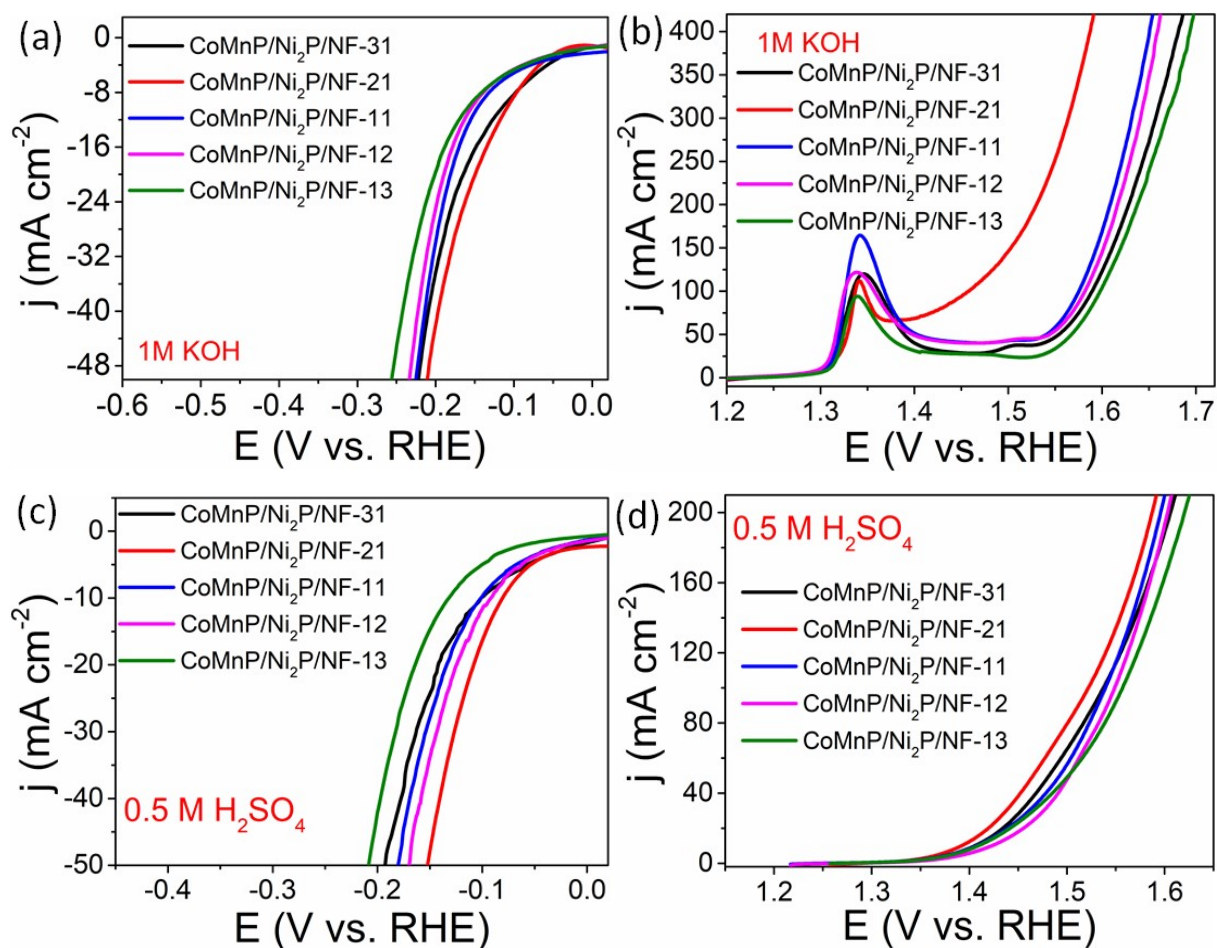
Fig. S8 (a) HER and (b) OER polarization curves of CoMnP/Ni$_2$P-NF-31, CoMnP/Ni$_2$P-NF-21, CoMnP/Ni$_2$P-NF-11, CoMnP/Ni$_2$P-NF-12, and CoMnP/Ni$_2$P-NF-13 in1M KOH. (c) HER and (d) OER polarization curves of CoMnP/Ni$_2$P-NF-31, CoMnP/Ni$_2$P-NF-21, CoMnP/Ni$_2$P-NF-11, CoMnP/Ni$_2$P-NF-12, and CoMnP/Ni$_2$P-NF-13 in 0.5 M H$_2$SO$_4$.
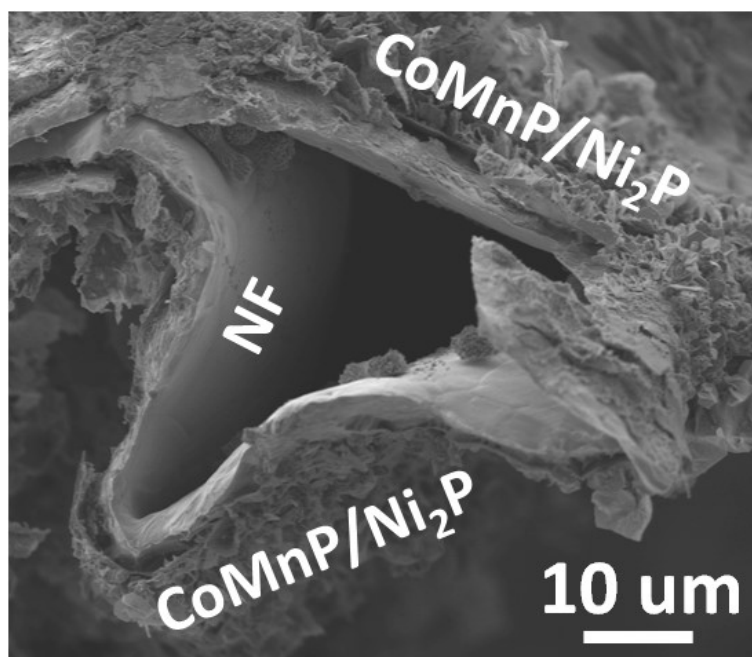
Fig. S9 Cross-section SEM image of CoMnP/Ni$_2$P/NF-21 (also named as CoMnP/Ni$_2$P/NF).
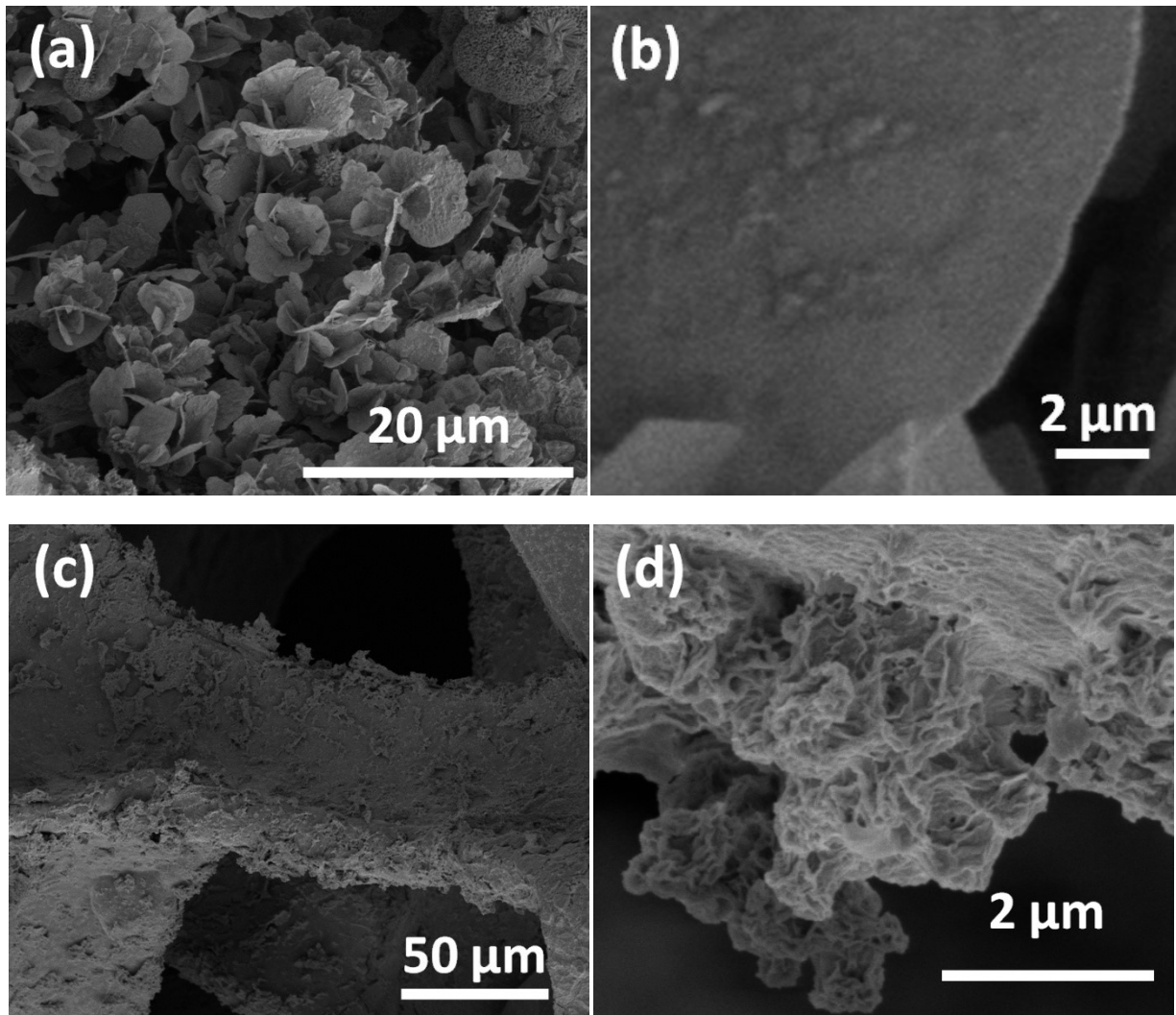
Fig. S10 SEM images of (a,b) CoP/Ni$_2$P/NF and (c,d) MnP/Ni$_2$P/NF.
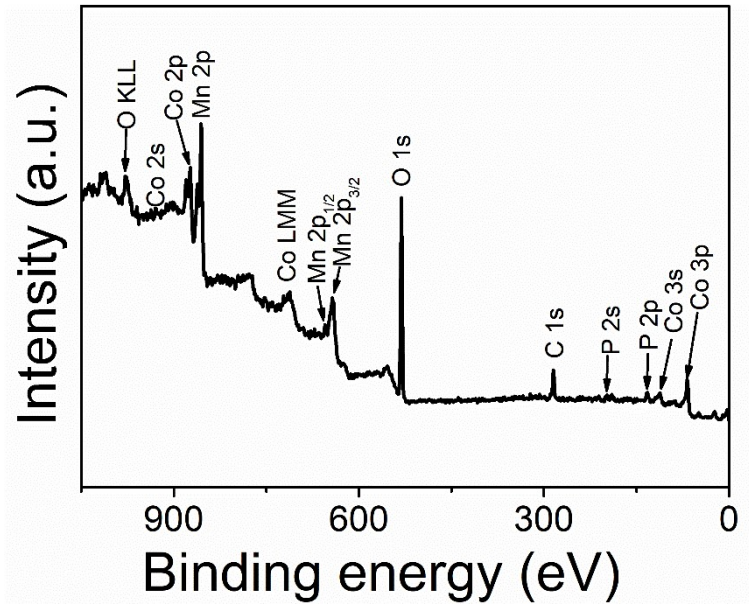
Fig. S11 XPS survey spectrum of CoMnP/Ni$_2$P/NF.
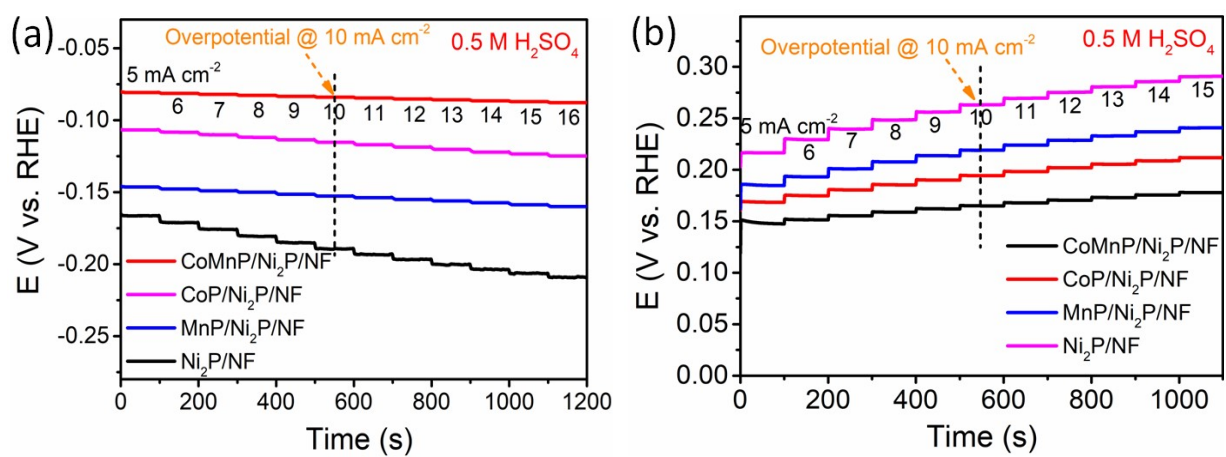
Fig. S12 Chronopotentiometric plots of (a) HER and (b) OER of the as-synthesized samples at different current densities in 0.5 M H_2SO_4.
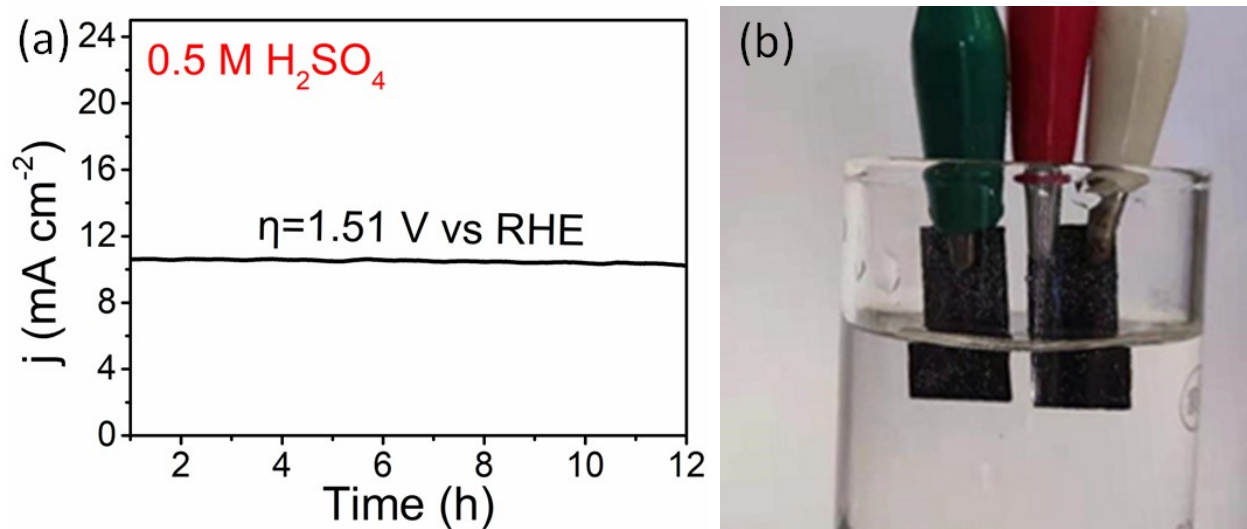
Fig. S13 (a) Chronoamperometric curve of CoMnP/Ni$_2$P/NF for water electrolysis at 1.51 V by using alligator clip to connect the NF catalyst directly to exclude the influence of Pt of the generally used Pt electrode holders on the catalytic performance. (b) Photograph of the electrochemical setup by using alligator clip to connect the NF catalyst directly for overall water splitting. The electrolyte is 0.5M H$_2$SO$_4$ (pH~0).
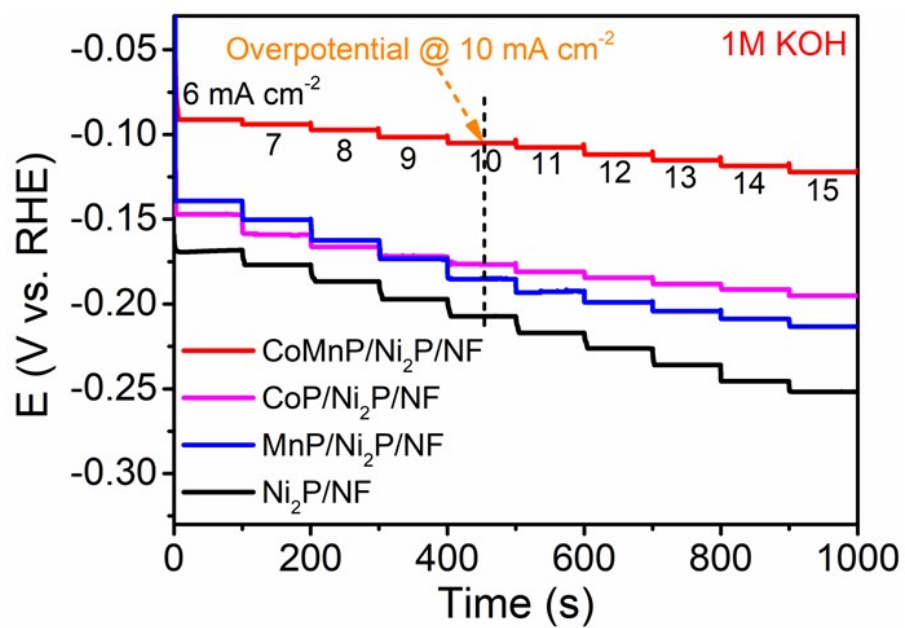
Fig. S14 Chronopotentiometric plots of HER of the samples at different current densities in 1 M KOH.
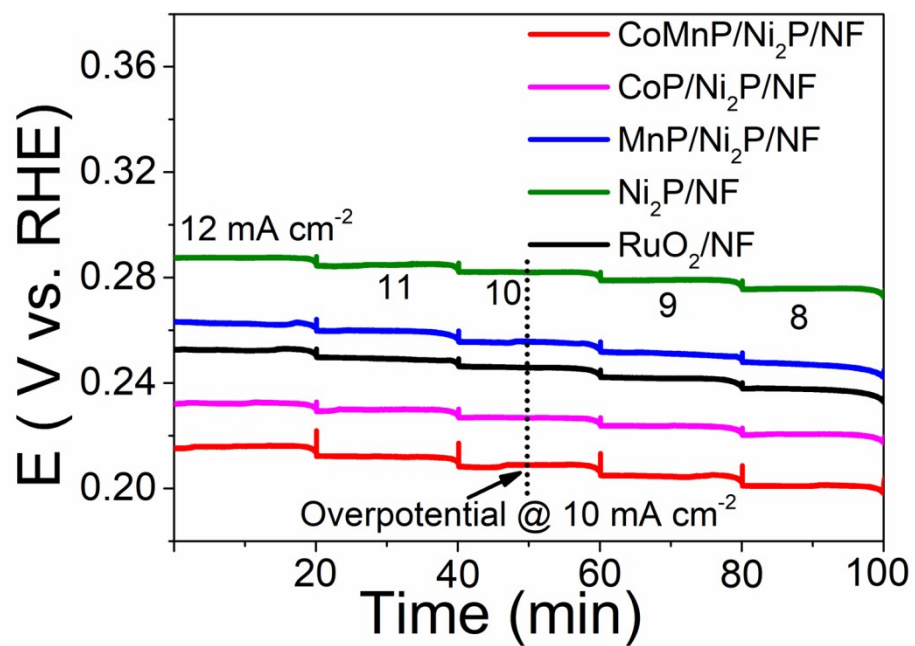
Fig. S15 Chronopotentiometric plots of OER of the samples at different current densities in 1 M KOH.
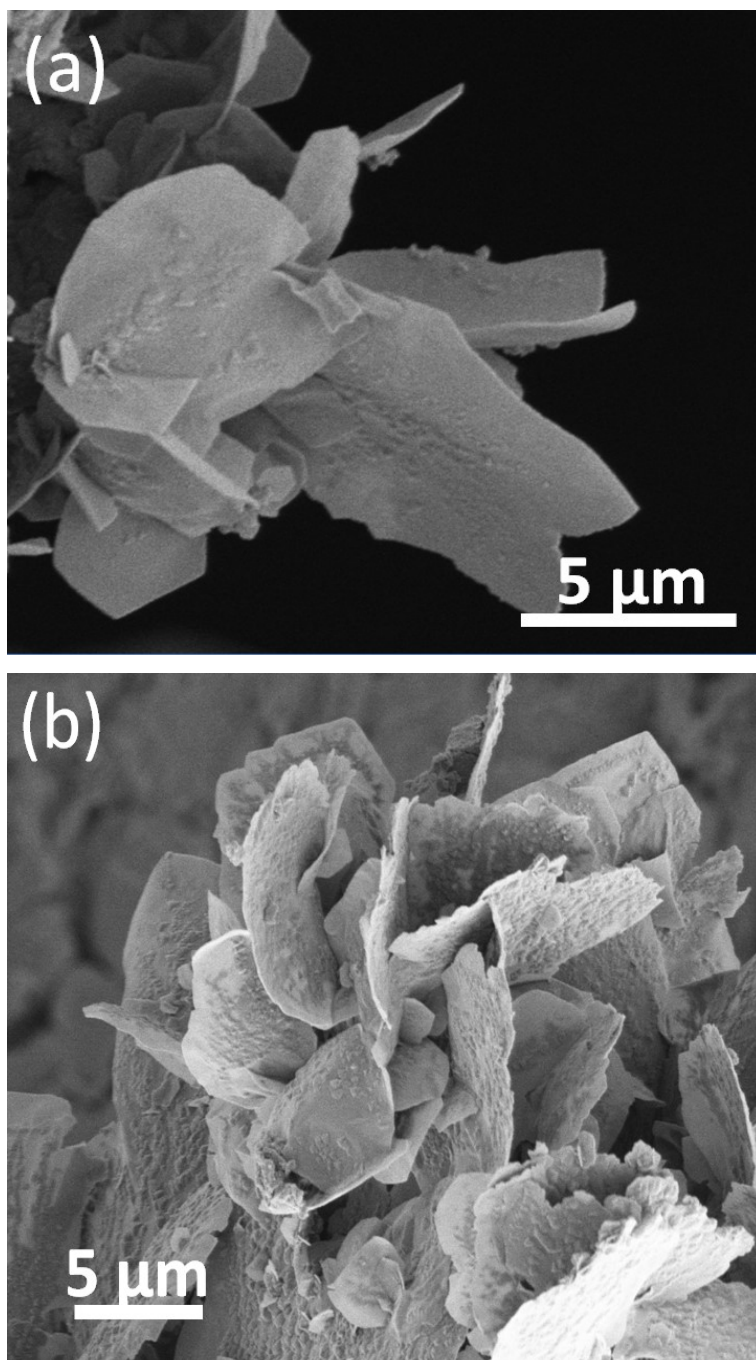
Fig. S16 SEM images of CoMnP/Ni$_2$P/NF after overall water splitting in 1.0 M KOH for 12 h: (a) Cathode and (b) Anode.
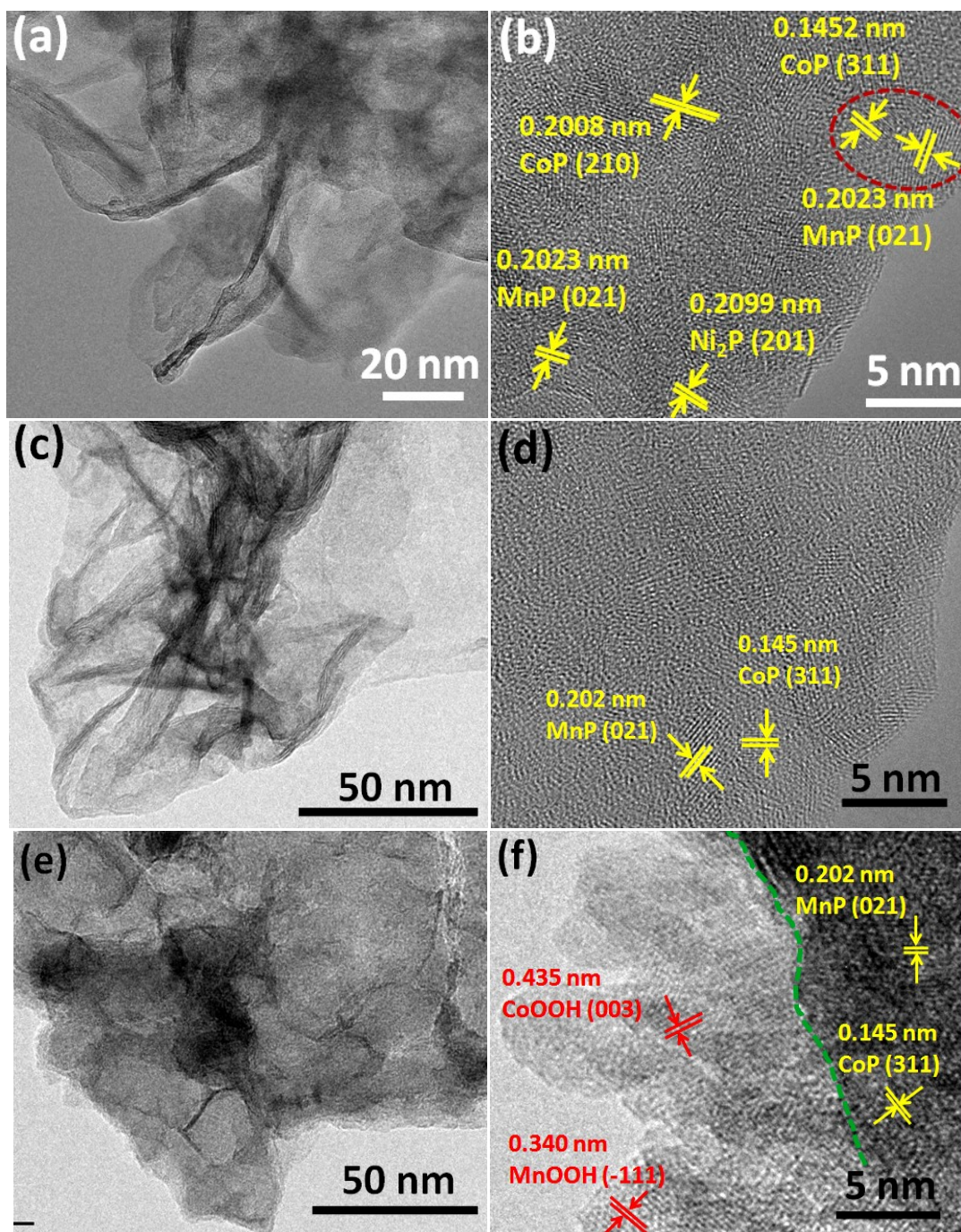
Fig. S17 (a,c,e) TEM and (b,d,f) HRTEM images of (a,b) fresh CoMnP/Ni$_2$P/NF catalyst and the (c,d) spent CoMnP/Ni$_2$P/NF catalyst (cathode), and (e,f) spent CoMnP/Ni$_2$P/NF catalyst (anode) after overall water splitting in 1.0 M KOH for 12 h.
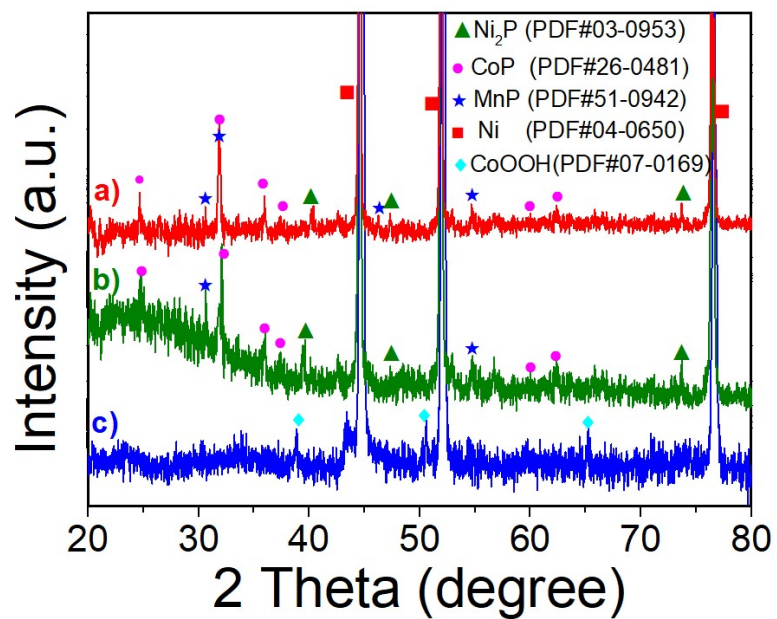
Fig. S18 XRD patterns of CoMnP/Ni$_2$P/NF after overall water splitting in 1.0 M KOH for 12 h: (a) Fresh CoMnP/Ni$_2$P/NF bifunctional electrode, (b) Spent CoMnp/Ni$_2$P/NF cathode and (c) Spent CoMnp/Ni$_2$P/NF anode.
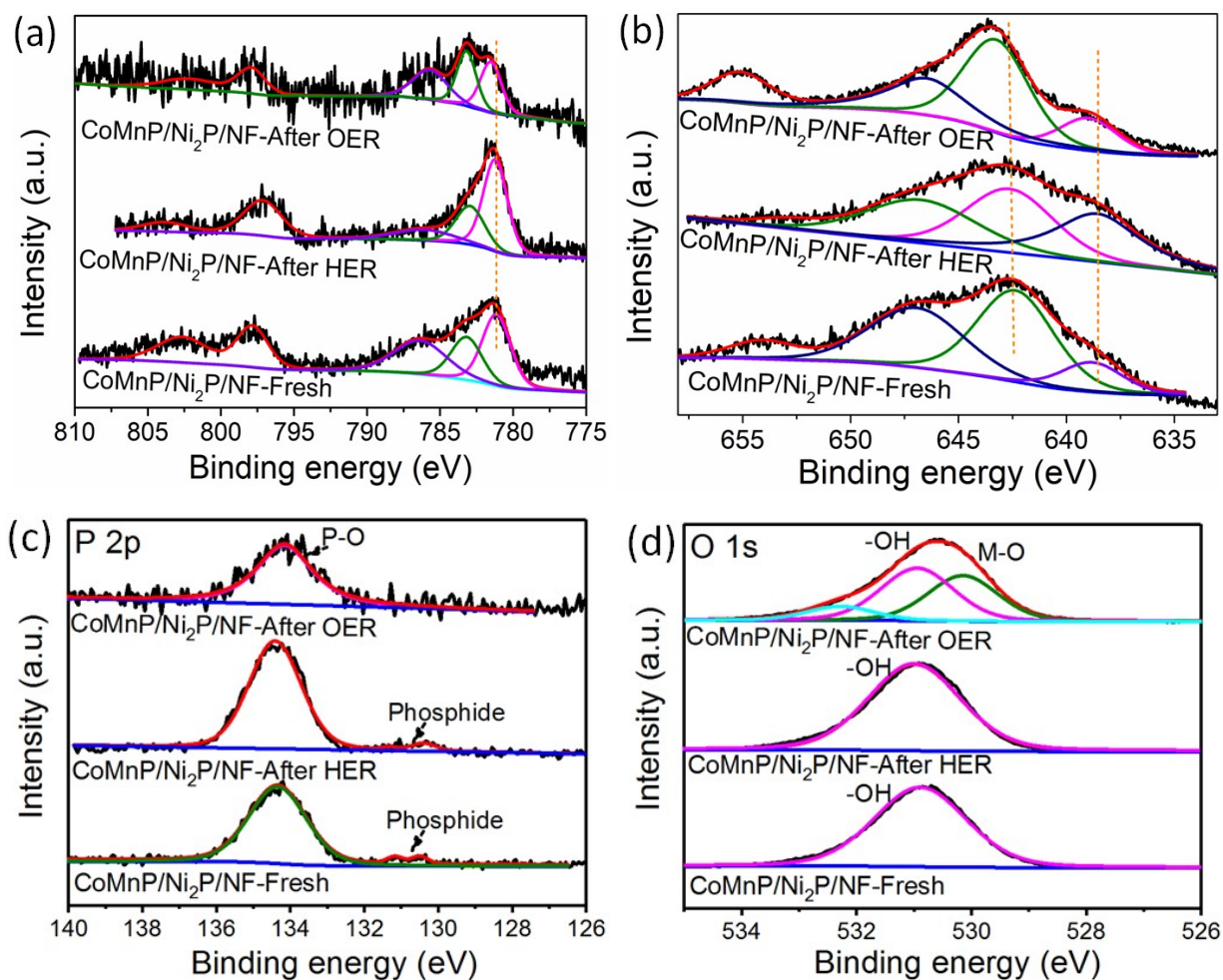
Fig. S19 High-resolution XPS spectra of (a) Co 2p and (b) Mn 2p, (c) O 1s and (d) P 2p of CoMnP/Ni$_2$P/NF after HER and OER for 24 h in 1 M KOH solution.
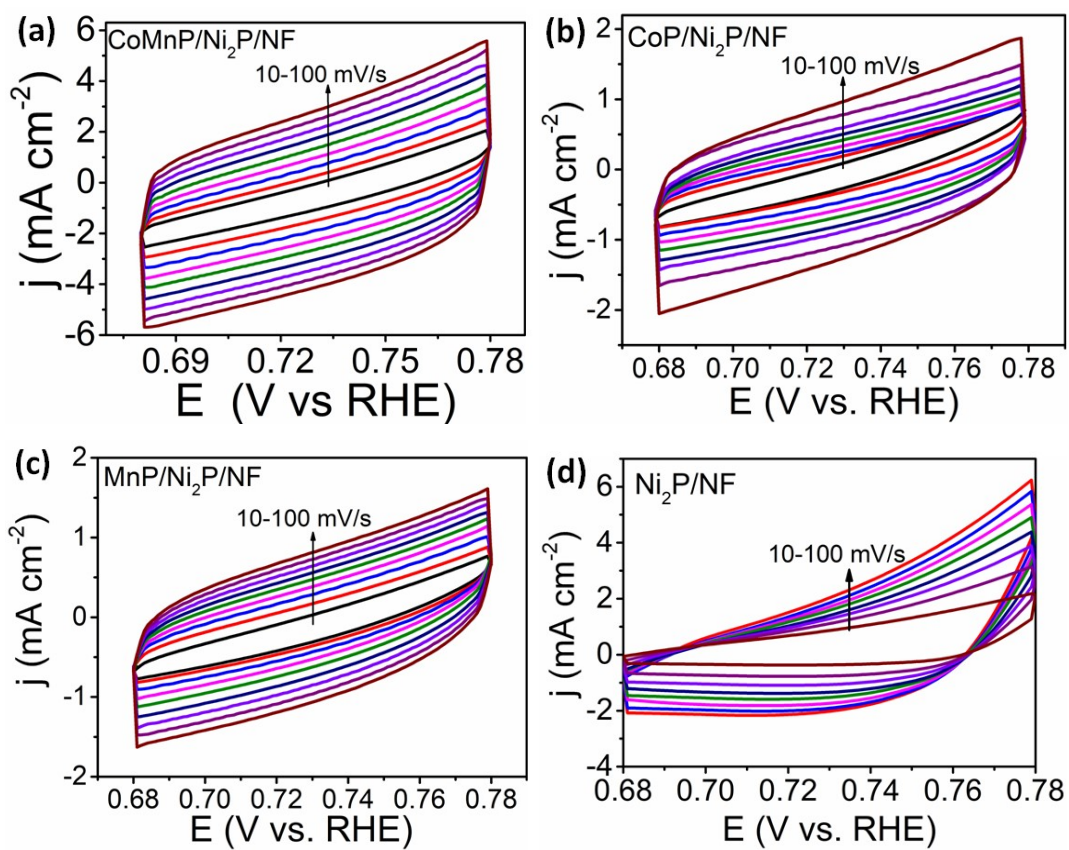
Fig. S20 Cyclic voltammograms at various scan rates of 10, 20, 30, 40, 50, 60, 70, 80 and 100 mV s^{-1} at η= 0.68-0.78 V vs RHE for (a) CoMnP/Ni$_2$P/NF, (b) CoP/Ni$_2$P/NF, (c) MnP/Ni$_2$P/NF, and (d) Ni$_2$P/NF.
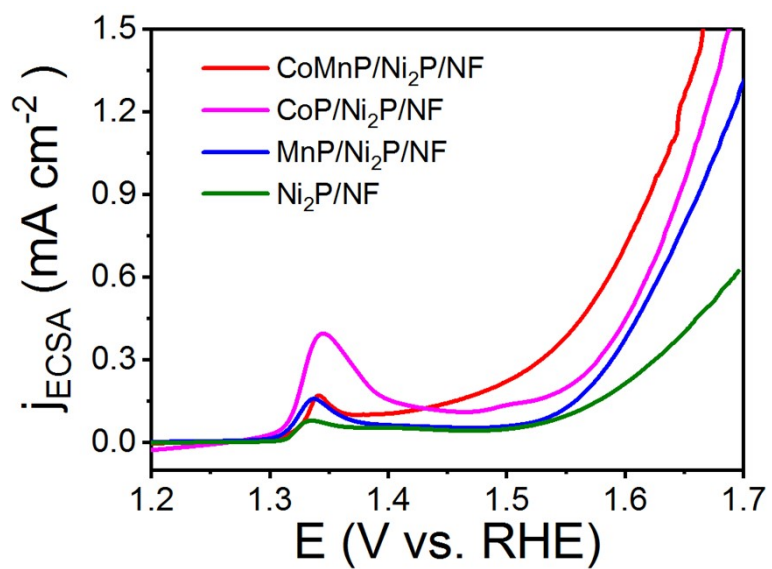
Fig. S21 Normalized polarizationcurves by ECSA for OER of CoMnP/Ni$_2$P/NF, CoP/Ni$_2$P/NF, MnP/Ni$_2$P/NF, and Ni$_2$P/NF in 1M KOH solution.
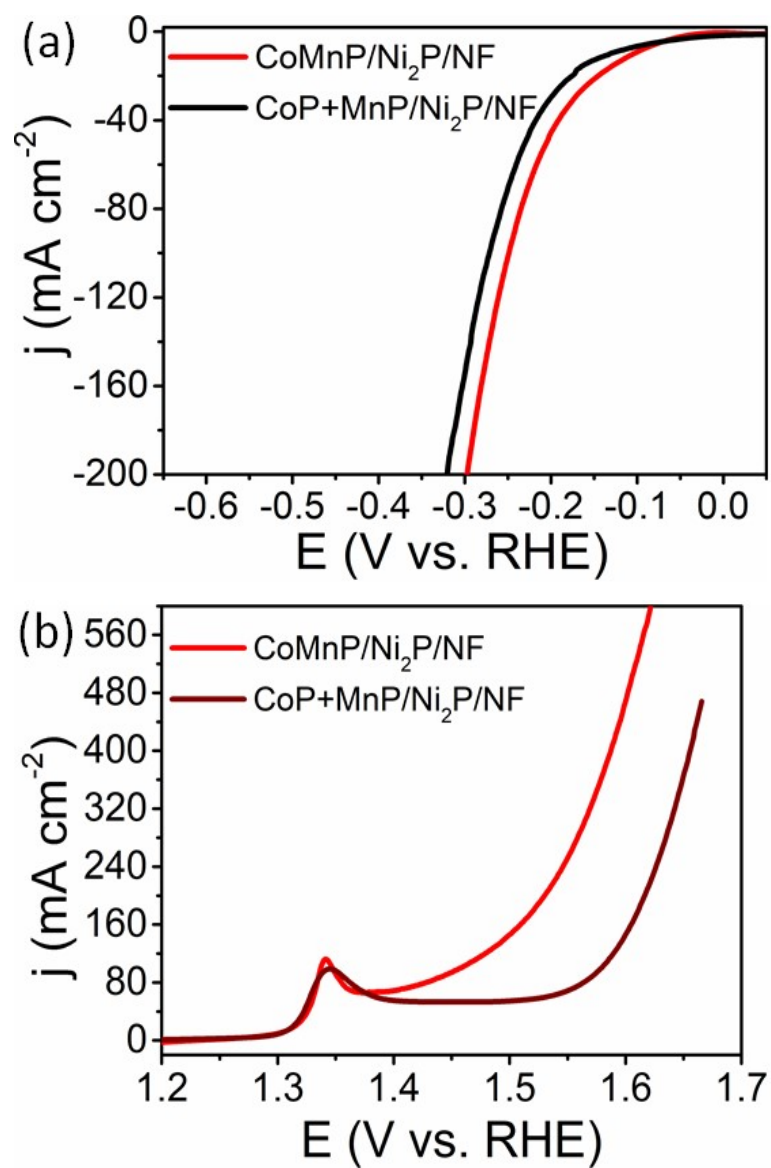
Fig. S22 (a) HER and (b) OER polarization curves of the CoMnP/Ni$_2$P/NF and CoP+MnP/Ni$_2$P/NF catalysts in 1M KOH.
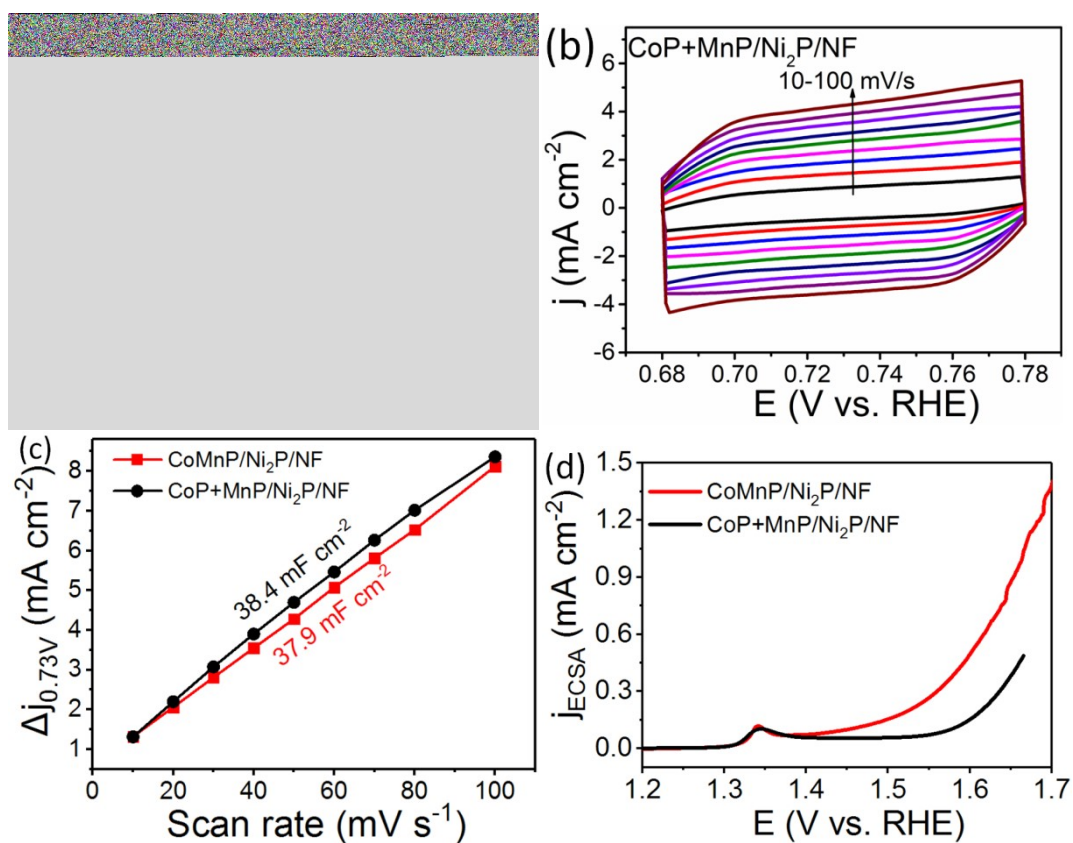
Fig. S23 (a,b) Cyclic voltammograms at various scan rates of 10, 20, 30, 40, 50, 60, 70, 80 and 100 mV s^{-1} at η= 0.68-0.78 V vs RHE for (a) CoMnP/Ni$_2$P/NF and (b) CoP+MnP/Ni$_2$P/NF. (c) Current density differences (Δj) as a function of scan rate and (d) normalized polarization curves by ECSA of CoMnP/Ni$_2$P/NF and CoP+MnP/Ni$_2$P/NF. The electrolyte is 1 M KOH (pH~14).
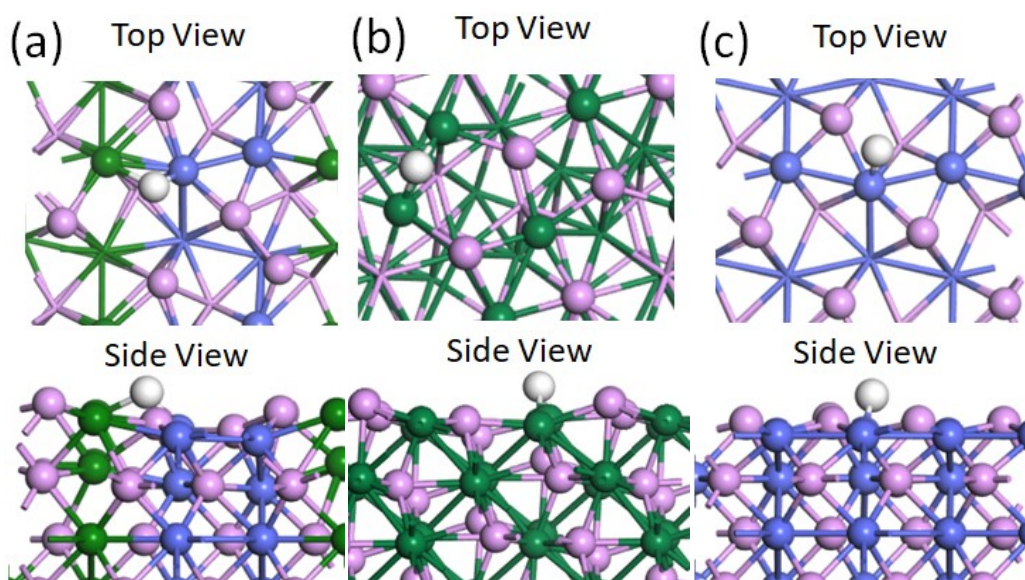
Fig. S24 Optimized models for *H intermediate of HER process on site of (a) CoMnP, (b) CoP, and (c) MnP. Color codes: blue (Co), pink (P), green (Mn), white (H).
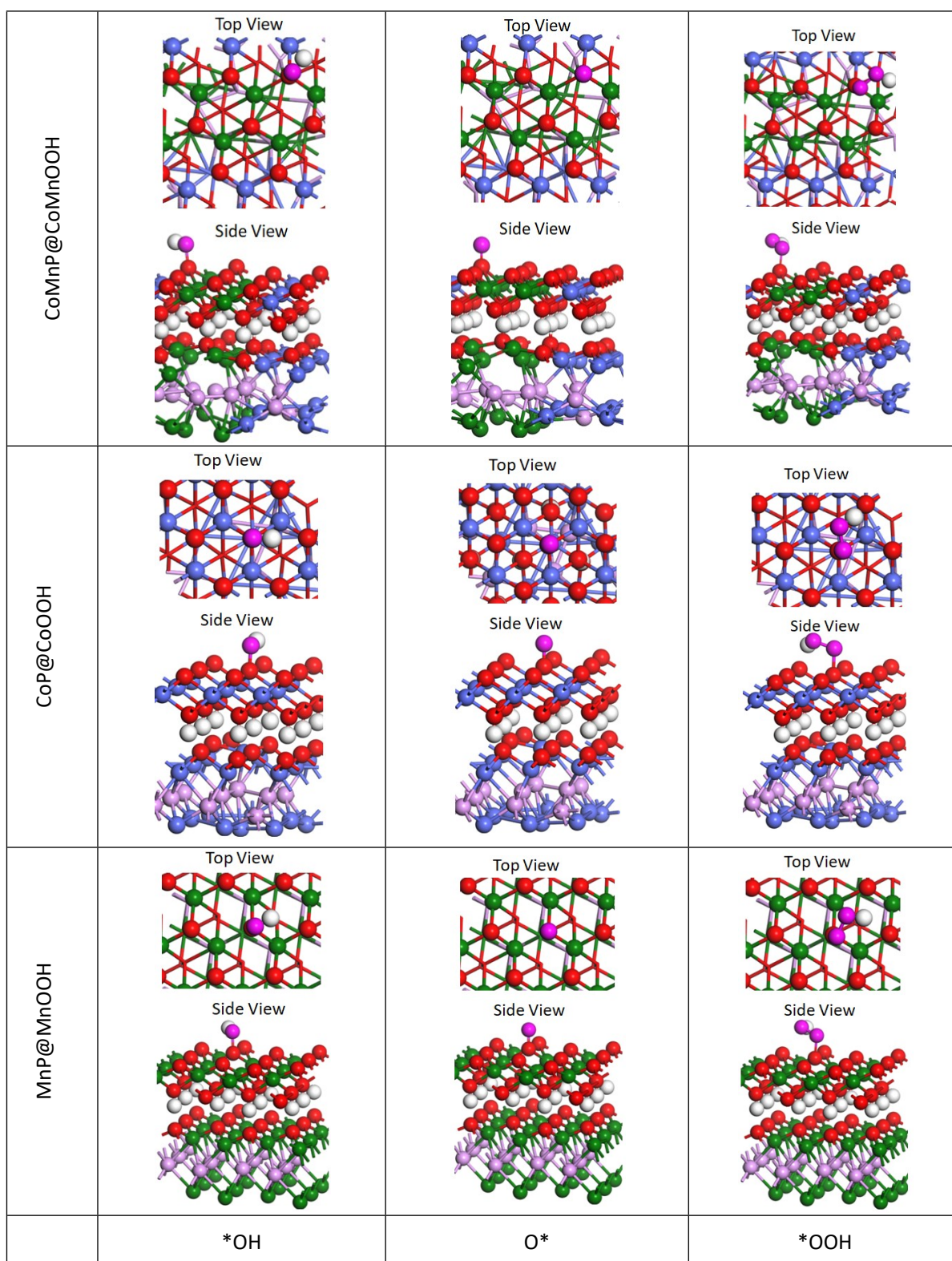
Fig. S25 Optimized models for *O, *OH, and *OOH intermediates of OER process on sites of (a) CoMnP@CoMnOOH, (b) CoP@CoOOH, and (c) MnP@MnOOH. Color codes: blue (Co), pink (P), green (Mn), white (H), red (oxygen of CoOOH or MnOOH) and magenta (oxygen of O*, OH* or OOH*).

2. Supplementary Tables

Table S1. Average mass loading of electrocatalysts on Ni foam (NF) current collector.

Samples	Mass loading (mg cm^{-2})
CoMnP/Ni$_2$P/NF-31	1.68
CoMnP/Ni$_2$P/NF-21 **(CoMnP/Ni$_2$P/NF)**	**1.62**
CoP+MnP/Ni$_2$P/NF	**1.69**
CoMnP/Ni$_2$P/NF-11	1.66
CoMnP/Ni$_2$P/NF-12	1.63
CoMnP/Ni$_2$P/NF-13	1.70
CoP/Ni$_2$P/NF	1.67
MnP/Ni$_2$P/NF	1.65
Ni$_2$P/NF	1.14
RuO$_2$	1.62
Pt/C	1.62

Table S2. ICP-AES data and the atomic ratio of Co/Mn of CoMnP/Ni$_2$P-NF-xy samples.

Samples	Feeding ratios of Co/Mn	C_{Co} (mg/L)	C_{Mn} (mg/L)	Atomic ratio of Co/Mn
CoMnP/Ni$_2$P/NF-31	3:1	0.43	0.15	2.70/1
CoMnP/Ni$_2$P/NF-21 **(CoMnP/Ni$_2$P/NF)**	**2:1**	**1.51**	**0.78**	**1.82/1**
CoMnP/Ni$_2$P/NF-11	1:1	0.70	0.69	1/0.95
CoMnP/Ni$_2$P/NF-12	1:2	2.36	4.28	1/1.95
CoMnP/Ni$_2$P/NF-13	1:3	1.42	3.95	1/2.98

Table S3. The C_{dl} and ECSA of the as-prepared samples.

Catalysts	C_{dl}(mF cm^{-2})	ECSA(cm^{-2})
CoMnP/Ni$_2$P/NF-31	22.05	551.25
CoMnP/Ni$_2$P/NF-21 **(CoMnP/Ni$_2$P/NF)**	**37.90**	**947.50**
CoP+MnP/Ni$_2$P/NF	38.40	960.00
CoMnP/Ni$_2$P/NF-11	20.93	523.25
CoMnP/Ni$_2$P/NF-12	19.58	489.50
CoMnP/Ni$_2$P/NF-13	14.79	369.75
CoP/Ni$_2$P/NF	16.50	412.50
MnP/Ni$_2$P/NF	14.30	357.50
Ni$_2$P/NF	9.70	242.50

Table S4. HER performance of the as-prepared samples in different electrolytes.

Catalysts	Overpotential in 1 M KOH (mV)		Overpotential in 0.5 M H$_2$SO$_4$ (mV)	
	10 mA cm^{-2}	100mA cm^{-2}	10 mA cm^{-2}	100mA cm^{-2}
CoMnP/Ni$_2$P/NF-31	138	291	101	234
CoMnP/Ni$_2$P/NF-21 **(CoMnP/Ni$_2$P/NF)**	**108**	**249**	**84**	**195**
CoMnP/Ni$_2$P/NF-11	148	268	102	224
CoMnP/Ni$_2$P/NF-12	150	276	92	216
CoMnP/Ni$_2$P/NF-13	158	301	132	249

Table S5. OER performance of the as-prepared samples in different electrolytes.

Catalysts	Overpotential in 1 M KOH at100 mA cm^{-2} (mV)	Overpotential in 0.5 M H$_2$SO$_4$ (mV)	
		10 mA cm^{-2}	100 mA cm^{-2}
CoMnP/Ni$_2$P/NF-31	360	176	308
CoMnP/Ni$_2$P/NF-21 (**CoMnP/Ni$_2$P/NF**)	**228**	**165**	**292**
CoMnP/Ni$_2$P/NF-11	346	178	310
CoMnP/Ni$_2$P/NF-12	352	194	319
CoMnP/Ni$_2$P/NF-13	369	180	327

Table S6. HER performance of the as-prepared samples in different electrolytes.

Catalysts	Overpotential in 1 M KOH (mV)		Overpotential in 0.5 M H$_2$SO$_4$ (mV)	
	10 mA cm^{-2}	100mA cm^{-2}	10 mA cm^{-2}	100mA cm^{-2}
CoMnP/Ni$_2$P/NF	**108**	**249**	**84**	**195**
CoP/Ni$_2$P/NF	178	302	118	251
MnP/Ni$_2$P/NF	187	325	153	272
Ni$_2$P/NF	206	341	192	339
Pt/C	51	--	38	--

Table S7. Comparison of HER performance of the developed hierarchical CoMnP/Ni$_2$P/NF electrocatalyst with reported electrocatalysts in literatures.

Electrolyte	Catalysts	Overpotential at 10 mA cm^{-2} (mV)	Ref.
1 M KOH	**CoMnP/Ni$_2$P/NF**	**108**	**This work**
	Hierarchical Ni-Co-P HNBs	107	1
	CoNiP@NF	155	2
	Co$_2$P/Co foil	157	3
	CoP/PNC	165	4
	Co$_{0.6}$Fe$_{0.4}$P$_{-1.125}$	133	5
	NiFeOH/CoS$_x$/NF	146	6
	Co$_1$Mn$_1$CH/NF	180	7
	Cu$_{0.3}$Co$_{2.7}$P/NC	220	8
	MoSe$_2$-CoSe$_2$	148	9
	Part-PhCo@Co–P@NPCNTs	160	10
	Co/β-Mo$_2$C@NCNTs	170	11
	CoMoNiS-NF-31	113	12
0.5 M H$_2$SO$_4$	**CoMnP/Ni$_2$P/NF**	**84**	**This work**
	MoP-C	136	13
	CoMoNiS-NF-31	103	12
	CoP NA/Ti	90	13
	CoP/NPC/TF	91	14
	NiCo$_2$Px/CF	104	15
	MoP@NC	142	16
	CoP/Ti	90	17

Table S8. OER performance of the as-prepared samples in different electrolytes.

Catalysts	OER (1 M KOH)		ꔯOER (0.5 M H_2SO_4)	
	10 (mA cm^{-2})	100 (mA cm^{-2})	10 (mA cm^{-2})	100 (mA cm^{-2})
CoMnP/Ni$_2$P/NF	**209**	**228**	**165**	**292**
CoP/Ni$_2$P/NF	227	366	195	325
MnP/Ni$_2$P/NF	255	375	224	338
Ni$_2$P/NF	282	423	265	388
RuO$_2$	246	319	184	321

Table S9. Comparison of OER performance of the developed hierarchical $CoMnP/Ni_2P/NF$ electrocatalyst with reported electrocatalysts in literatures.

Electrolyte	Catalysts	Overpotential at 10 mA cm^{-2} (mV)	Ref.
1 M KOH	**CoMnP/Ni$_2$P/NF**	**209**	**This work**
	Co$_2$P/Co foil	319	3
	CoP/PNC	300	4
	Fe-CoP/Ti	230	18
	Co$_{0.6}$Fe$_{0.4}$P-$_{1.125}$	298	19
	CoP/N-dopedCNT polyhedron	310	20
	Part-PhCo@Co–P@NPCNTs	290	21
	Cobalt Oxide Layers	370	22
	Fe-CoP/CoO	219	23
	NiCoFeP/C	270	24
	NiCoP/CC	242	25
	Ni$_2$P/Ni/NF	200	26
	NiCo$_2$S$_4$ NW/NF	260	27
	Ni$_2$P-VP$_2$/NF	220	28
	CoMoNiS-NF-31	166	12
0.5 M H$_2$SO$_4$	**CoMnP/Ni$_2$P/NF**	**165**	**This work**
	NC-CNT/CoP/CC	350	29
	N-WC/CFP	220	30
	CoMoNiS-NF-31	228	12
0.1 M HClO$_4$	CNx	260	31
	Co$_2$P	220	32

Table S10: Comparison of the electrocatalytic performance of the developed hierarchical $CoMnP/Ni_2P/NF$ electrocatalyst with reported electrocatalysts in literatures.

Electrolyte	Catalysts	Cell voltage at 10 mA cm^{-2} (V)	Ref.
1 M KOH	**CoMnP/Ni$_2$P/NF**	**1.54**	**This work**
	CC-NC-NiFeP	1.54	33
	NiP/Ni/NF	1.49	26
	NiCoP	1.52	25
	CoP/N-dopedCNT polyhedron	1.64	20
	Part-PhCo@Co–P@NPCNTs	1.63	21
	NiCoFeP/C	1.60	24
	NiCo$_2$S$_4$ NW/NF	1.63	27
0.5 M H$_2$SO$_4$	**CoMnP/Ni$_2$P/NF**	**1.43**	**This work**
	NC-CNT/CoP/CC	1.66	29
	Co/CoP	1.89	34
	Ni-Mo-P	1.52	35
	NiAlP	1.73	36
	Co-MoS$_2$	1.90	37
	CoMoNiS-NF-31	1.47	12

3. References

1. Hu, E., Feng, Y., Nai, J., Zhao, D., Hu, Y., Lou, X. W. Construction of Hierarchical Ni–Co–P Hollow Nanobricks with Oriented Nanosheets for Efficient Overall Water Splitting. *Energy Environ. Sci.*, 2018, **11**, 872-880.

2. Han, A., Chen, H., Zhang, H., Sun, Z., Du, P. Ternary Metal Phosphide Nanosheets as a Highly Efficient Electrocatalyst for Water Reduction to Hydrogen Over a Wide pH Range from 0 to 14. *J. Mater. Chem. A.,* 2016*,* **4***,* 10195-10202.

3. Yuan, C. Z., Zhong, S. L., Jiang, Y. F., Yang, Z. K., Zhao, Z. W., Zhao, S. J., Jiang, N., Xu, A. W. Direct Growth of Cobalt-rich Cobalt Phosphide Catalysts on Cobalt Foil: An Efficient and Self-supported Bifunctional Electrode for Overall Water Splitting in Alkaline Media. *J. Mater. Chem. A.*, 2017, **5**, 10561-10566.

4. Z. Peng, Y. Yu, D. Jiang, Y. Wu, B. Xia, Z. Dong,N-doped Carbon Shell Coated CoP Nanocrystals Encapsulated in Porous N-doped Carbon Substrate as Efficient Electrocatalyst of Water Splitting. *Carbon,* 2019*,* **14**4, 464-471.

5. Lian, Y. B., Sun, H., Wang, X., Qi, P., Mu, Q., Chen, Y., Ye, J., Zhao, X., Deng, Z., Peng, Y. Carved Nanoframes of Cobalt–iron Bimetal Phosphide as a Bifunctional Electrocatalyst for Efficient Overall Water Splitting. *Chem. Sci.,* 2019*,* **10**, 464-474.

6. Bose, R., Jothi, V. R., Karuppasamy, K., Alfantazi, A.,Yi, S. C.High Performance Multicomponent Bifunctional Catalysts for Overall Water Splitting. *J. Mater. Chem. A,* 2020*,* **8**, 13795–13805.

7. Tang, T., Jiang, W., Niu, S., Liu, N., Luo, H., Chen, Y., Jin, S., Gao, F., Wan, L., Hu, J. Electronic and Morphological Dual Modulation of Cobalt Carbonate Hydroxides by Mn Doping toward Highly Efficient and Stable Bifunctional Electrocatalysts for Overall Water Splitting. *J. Am. Chem. Soc.*, 2017, **139**, 8320–8328.

8. Song, J. H., Zhu, C., Xu, B. Z., Fu, S., Engelhard, M. H., Ye, R., Du, D., Beckman, S., Lin, Y. Bimetallic Cobalt-Based Phosphide Zeolitic Imidazolate Framework: CoP_x Phase-Dependent Electrical Conductivity and Hydrogen Atom Adsorption Energy for Efficient Overall Water Splitting. *Adv. Energy Mater.*, 2017, **7**, 1601555.

9. Wang, X. Q., Zheng, B., Yu, B., Wang, B., Hou, W., Zhang, W., Chen,Y. In Situ Synthesis of Hierarchical $MoSe_2$–$CoSe_2$ Nanotubes as an Efficient Electrocatalyst for the Hydrogen Evolution Reaction in both Acidic and Alkaline Media. *J. Mater. Chem. A,* 2018*,* **6**, 7842–7850.

10. Jiao, J. Q., Yang, W., Pan, Y., Zhang, C., Liu, S., Chen, C., Wang, D. Interface Engineering of Partially Phosphidated Co@Co–P@NPCNTs for Highly Enhanced Electrochemical Overall Water Splitting. *Small,* 2020, **16**, 2002124.

11. Ouyang, T., Ye, Y., Wu, C., Xiao, K., Liu, Z. Heterostructures Composed of N-Doped Carbon Nanotubes Encapsulating Cobalt and β-Mo_2C Nanoparticles as Bifunctional Electrodes for Water Splitting. *Angew. Chem. Int. Ed.,* 2019, **58**, 4923 –4928.

12. Yang, Y., Yao, H., Yu, Z., Islam, S. M., He, H., Yuan, M., Yue, Y., Xu, K., Hao, W., Sun, G., Li, H., Ma, S., Zapol, P.,

Kanatzidis, M.Hierarchical Nanoassembly of $MoS_2/Co_9S_8/Ni_3S_2$/Ni as a Highly Efficient Electrocatalyst for Overall Water Splitting in a Wide pH Range. *J. Am. Chem. Soc.*, 2019, **141**, 10417–10430.

13. Wu, Z. X., Wang, J., Liu, R., Xia, K., Xuan, C., Guo, J., Lei, W., Wang, D.Facile Preparation of Carbon Sphere Supported Molybdenum Compounds (P, C and S) as Hydrogen Evolution Electrocatalysts in Acid and Alkaline Electrolytes. *Nano Energy*, 2017, **32**, 511–519.

14. Huang, X., Xu, X., Li, C., Wu, D., Cheng, D., Cao, D. Vertical CoP Nanoarray Wrapped by N,P-Doped Carbon for Hydrogen Evolution Reaction in Both Acidic and Alkaline Conditions. *Adv. Energy Mater*., 2019,**9**, 1803970.

15. Zhang, R.; Wang, X.; Yu, S.; Wen, T.; Zhu, X.; Yang, F.; Sun, X.; Wang, X.; Hu, W. Ternary NiCo2Px Nanowires as pH-Universal Electrocatalysts for Highly Efficient Hydrogen Evolution Reaction. *Adv. Mater*., 2017, **29**, 1605502.

16. Gao, S.; Liu, Y.; Lia, G.; Guo, Y.; Zou, Y.; Zou, X.General Urea-assisted Synthesis of Carbon-coated Metal Phosphide Nanoparticles for Efficient Hydrogen Evolution Electrocatalysis. *Electrochim. Acta*, **2016**, 199, 99–107.

17. Pu, Z. H., Liu, Q., Jiang, P., Asiri, A. M., Obaid, A. Y., Sun, X.CoP Nanosheet Arrays Supported on a Ti Plate: An Efficient Cathode for Electrochemical Hydrogen Evolution. *Chem. Mater*., 2014, **26**, 4326–4329.

18. Tang, C., Zhang, R., Lu, W., He, L., Jiang, X., Asiri, A. M., Sun, X. Fe-Doped CoP Nanoarray: A Monolithic Multifunctional Catalyst for Highly Efficient Hydrogen Generation. *Adv. Mater*., 2017, **29**, 1602441.

19. Lian, Y., Sun, H., Wang, X., Qi, P., Mu, Q., Chen, Y., Ye, J., Zhao, X., Deng, Z., Peng,Y. Carved Nanoframes of Cobalt–iron Bimetal Phosphide as a Bifunctional Electrocatalyst for Efficient Overall Water Splitting. *Chem. Sci*., 2019, **10**, 464–474.

20. Pan, Y., Sun, K., Liu, S., Cao, X., Wu, K., Cheong, W., Chen, Z., Wang, Y., Li, Y., Liu, Y., Wang, D., Peng, Q., Chen, C., Li, Y. Core−Shell ZIF-8@ZIF-67-Derived CoP Nanoparticle-Embedded N-Doped Carbon Nanotube Hollow Polyhedron for Efficient Overall Water Splitting. *J. Am. Chem. Soc.*, 2018, **140**, 2610–2618.

21. Jiao, J.; Yang, W.; Pan, Y.; Zhang, C.; Liu, S.; Chen, C.; Wang,D. Interface Engineering of Partially Phosphidated Co@Co–P@NPCNTs for Highly Enhanced Electrochemical Overall Water Splitting. *Small*, 2020, **16**, 2002124.

22. Zhou, T., Xu, W., Zhang, N., Du, Z.; Zhong, C., Yan, W., Ju, H., Chu, W., Jiang, H., Wu, C., Xie, Y.Ultrathin Cobalt Oxide Layers as Electrocatalysts for High-Performance Flexible Zn–Air Batteries. *Adv. Mater*., 2019, **31**, 1807468.

23. Guo, M. J., Song, S., Zhang, S., Yan, Y., Zhan, K., Yang, J., Zhao, B. Fe-Doped Ni–Co Phosphide Nanoplates with Planar Defects as an Efficient Bifunctional Electrocatalyst for Overall Water Splitting. *ACS Sust. Chem. Eng*., 2020, **8**, 7436−7444.

24. Wei, X. J., Zhang, Y., He, H., Peng, L., Xiao, S., Yao, S., Xiao, P.Carbon-incorporated Porous Honeycomb NiCoFe Phosphide Nanospheres Derived from a MOF Precursor for Overall Water Splitting. *Chem. Commun*., 2019, **55**, 10896-10899.

25. Du, C., Yang, L., Yang, F., Cheng, G., Luo, W.Nest-like NiCoP for Highly Efficient Overall Water Splitting. *ACS Catal*., 2017,**7**, 4131–4137.

26. You, B., Jiang, N., Sheng, M., Bhushan, M. W., Sun,Y. Hierarchically Porous Urchin-Like Ni2P Superstructures Supported on Nickel Foam as Efficient Bifunctional Electrocatalysts for Overall Water Splitting. *ACS Catal.*, 2016, **6**, 714–721.

27. Sivanantham, A., Ganesan, P., Shanmugam, S. Hierarchical NiCo$_2$S$_4$ Nanowire Arrays Supported on Ni Foam: An Efficient and Durable Bifunctional Electrocatalyst for Oxygen and Hydrogen Evolution Reactions. *Adv. Funct. Mater*. , 2016, **26**, 4661–4672.

28. Yan, H. J., Xie, Y., Wu, A., Cai, Z., Wang, L., Tian, C., Zhang, X., Fu,H. Anion-Modulated HER and OER Activities of 3D Ni–V–Based Interstitial Compound Heterojunctions for High-Efficiency and Stable Overall Water Splitting. *Adv. Mater.*, 2019,**31**, 1901174.

29. Guan, C., Wu, H., Ren, W., Yang, C., Liu, X., Ouyang, X., Song, Z., Zhang, Y., Pennycook, S. J., Cheng, C., Wang, J.Metal–organic Framework-derived Integrated Nanoarrays for Overall Water Splitting. *J. Mater. Chem. A*, 2018, **6**, 9009–9018.

30. Han, N. N., Yang, K. R., Lu, Z., Li, Y., Xu, W., Gao, T., Cai, Z., Zhang, Y., Batista, V. S., Liu, W., Sun, X.Nitrogen-doped Tungsten Carbide Nanoarray as an Efficient Bifunctional Electrocatalyst for Water Splitting in Acid. *Nat. Commun.*, 2018, **9**, 924.

31. Mamtani, K., Jain, D., Dogu, D., Gustin, V., Gunduz, S., Co, A. C., Ozkan, U. S. Insights into Oxygen Reduction Reaction (ORR) and Oxygen Evolution Reaction (OER) Active Sites for Nitrogen-doped Carbon Nanostructures (CNx) in Acidic Media. *Appl. Catal. B: Environ*., 2018,**220**, 88–97.

32. Parra-Puerto, A., Ng, K. L., Fahy, K., Goode, A. E., Ryan, M. P., Kucernak, A.Supported Transition Metal Phosphides: Activity Survey for HER, ORR, OER, and Corrosion Resistance in Acid and Alkaline Electrolyte. *ACS Catal.*, 2019, **9**, 11515–11529.

33. Bian, J. L., Song, Z., Li, X., Zhang, Y., Cheng, C.Nickel Iron Phosphide Ultrathin Nanosheets Anchored on Nitrogen-doped Carbon Nanoflake Arrays as a Bifunctional Catalyst for Efficient Overall Water Splitting. *Nanoscale,* 2020, **12**, 8443–8452.

34. Xue, Z. H., Su, H., Yu, Q., Zhang, B., Wang, H., Li, X., Chen, J.Janus Co/CoP Nanoparticles as Efficient Mott–Schottky Electrocatalysts for Overall Water Splitting in Wide pH Range. *Adv. Energy Mater.*, 2017, **7**, 1602355.

35. Lai, C. G., Liu, X., Wang, Y., Cao, C., Yin, Y., Yang, H., Qi, X., Zhong, S., Hou, X., Liang, T. Modulating Ternary Mo–Ni–P by Electronic Reconfiguration and Morphology Engineering for Boosting all-pH Electrocatalytic Overall Water Splitting. *Electrochim. Acta,* 2020, **330**, 135294.

36. Cheng, W., Zhang, H., Zhao, X., Su, H., Tang, F., Tian, J., Liu, Q. A Metal-vacancy-solid-solution NiAlP Nanowall Array Bifunctional Electrocatalyst for Exceptional all-pH Overall Water Splitting. *J. Mater. Chem. A,* 2018, **6**, 9420-9427.

37. Xiong, Q. Z., Zhang, X., Wang, H., Liu, G., Wang, G., Zhang, H., Zhao, H.One-step Synthesis of Cobalt-doped MoS$_2$ Nanosheets as Bifunctional Electrocatalysts for Overall Water Splitting Under both Acidic and Alkaline Conditions. *Chem. Commun.*, 2018, **54**, 3859-3862.